Wang, L.; Snihirova, D.; Deng, M.; Vaghefinazari, B.; Lamaka, S.; Höche, D.; Zheludkevich, M.:

Tailoring electrolyte additives for controlled Mg-Ca anode activity in aqueous Mg-air batteries.

In: Journal of Power Sources. Vol. 460 (2020) 228106.

First published online by Elsevier: 05.04.2020

https://dx.doi.org/10.1016/j.jpowsour.2020.228106

Tailoring electrolyte additives for controlled Mg-Ca anode activity in aqueous Mg-air batteries

Linqian Wang[a,*], Darya Snihirova[a], Min Deng[a], Bahram Vaghefinazari[a], Sviatlana V. Lamaka[a], Daniel Höche[a], Mikhail L. Zheludkevich[a,b]

[a] *MagIC—Magnesium Innovation Center, Helmholtz-Zentrum Geesthacht (HZG), 21502 Geesthacht, Germany*

[b] *Institute of Materials Science, Faculty of Engineering, Kiel University, 24143 Kiel, Germany*

Abstract: Aqueous primary Mg-air batteries exhibit many merits as potential energy storage and conversion devices. In this work, the discharge performance of water based Mg-air batteries with advanced Mg-Ca anode was boosted by adding Mg^{2+} complexing agents into the electrolyte. The effect of electrolyte additives on the corrosion behavior and discharge properties of micro-alloyed Mg-Ca anode was investigated via hydrogen evolution test and half-cell discharge test. Electrochemical impedance spectroscopy (EIS) was performed to evaluate the effect of different electrolyte additives on the discharge activity of Mg-Ca anode. Basic characteristics of aqueous Mg-air battery in selected additive solution were tested and compared to pure NaCl solution. The results show that the addition of dedicated Mg^{2+} complexing agents can efficiently increase the discharge voltage and specific energy of respective Mg-air batteries. At 0.5 mA cm^{-2}, the discharge voltage reaches 1.86 V with regard to the cell containing 0.1 M 5-Sulfosalicylate, which is 270 mV higher than the discharge voltage in bulk 3.5 wt. % NaCl. The highest specific energy for the tested system is above 3.0 kWh kg^{-1} in NaCl solution with 0.1 M citrate at 1 mA cm^{-2} discharge current density.

Key words: Aqueous primary Mg-air battery; Electrolyte additives; Mg^{2+} complexing agent; Discharge performance; Chunk effect.

* Corresponding author.
E-mail address: Linqian.Wang@hzg.de (L. Wang), Telephone number: +49 (0)4152 871906, Postal address: Helmholtz-Zentrum Geesthacht, Max-Planck-Str. 1, 21502 Geesthacht, Germany.

1. Introduction

Aqueous primary Mg-air batteries can be adopted as attractive electrochemical energy storage and conversion devices because of superior discharge performance, safety, low cost, and environmental amiability [1-3]. Mg-air batteries consume oxygen from the air and the electrolyte as cathodic reactant, which is environmentally friendly and beneficial for the weight reduction of battery system, increasing the specific energy. Besides, water based Mg-air batteries can be artificially recharged through displacing anode material, which makes them as promising candidates for portable devices, remote devices, marine applications and military technologies [4].

As anode material, Mg exhibits highly negative standard electrode potential (-2.37 V vs SHE) and high volumetric capacity, which is even higher than that of Li (3833 mA h cm^{-3} for Mg vs. 2046 mA h cm^{-3} for Li) [1, 5-7]. However, during the discharge process, Mg anode materials suffer from serious self-corrosion, like micro-galvanic corrosion provoked by impurities or second phases, and chunk effect caused by the detachment of metallic particles from the anode surface as well as the accelerated corrosion due to negative difference effect [8, 9]. These side reactions significantly decrease the anode utilization efficiency and consequently reduce the battery capacity. Meanwhile, Mg anode surface is typically covered by discharge products, such as $Mg(OH)_2$ and MgO, which hinder the contact of the reactive surface with the electrolyte, and thus, decrease the discharge voltage [10]. Therefore, the actual discharge performance of Mg anode shifts far away from the theoretical value, adversely affecting the working voltage and practical specific energy of Mg-air batteries.

The possible technical solutions to diminish the difference between the theoretical and practical discharge performance of the studied Mg-air batteries are the modification of the anode and the optimization of the electrolyte composition. Numerous published works have focused on increasing the discharge performance of Mg-air batteries by looking for suitable Mg anode materials, which possess high discharge activities and low corrosion rates [10-14]. Aiming at improving the discharge performance of Mg anode materials, a lot of researchers put emphasis on alloying Mg with various metallic elements, such as, Al, Zn, Li, Mn, Ga, Pb, Hg, rare earth, etc. [15-21]. These metallic elements are in favor of the inhibition of the parasitic side reactions and the improvement of discharge potential

due to activation or their own electronegativity. Meanwhile, the addition of alloying elements improves the deformability of Mg alloy, which is also an important issue considering their practical application in Mg-air batteries [22-26]. However, some alloying elements are toxic, not economically relevant and demonstrate a low efficiency in enhancing the discharge performance. Recently, Deng et al. [27] proposed a newly developed Mg-Ca binary alloy as the anode material for Mg-air battery. Ca is an environmentally friendly and cost-effective alloying element. Upon addition of minor amount of Ca, the anode material gains higher discharge voltage and increased specific energy. Beside of alloy composition optimization, improving the microstructure of Mg anode materials by adopting deformation methods (such as extrusion and rolling) and heat treatments (such as normalizing, solid solution annealing and aging) also attracts attention of many researchers [28-31].

In addition to the modification of anode materials, the introduction of additives into electrolyte can also effectively improve the discharge performance of Mg-air batteries. One way to improve Mg-air battery performance is using corrosion inhibitors of Mg as electrolyte additives to obtain higher utilization efficiency [32-34]. However, the addition of traditional corrosion inhibitors normally does not improve the discharge voltage or makes it even worse. Recently, research work of Höche et al. [35, 36] showed that the self-corrosion of Mg could be decreased through hindering the re-deposition of iron. The utilization efficiency of commercially pure Mg (220 ppm Fe) doubled while the battery voltage of Mg-air battery increased by adopting salicylate as electrolyte additive at 0.5 mA cm^{-2}. Nevertheless, the utilization efficiency of commercially pure Mg in NaCl solution with salicylate is 27.2%. Some researchers also try to adopt surfactants with long chain as electrolyte additives [37, 38]. By the physical adsorption mechanism of surfactant, the corrosion rate of Mg anode would be decreased. According to the research work of Deyab [38], decyl glucoside as electrolyte additive can increase the utilization efficiency of pure Mg anode as well as improve its operating voltage. Whereas, this paper puts emphasis on the corrosion efficiency of decyl glucoside and dose not clarify the reason for the improvement of operating voltage.

This work aims to enhance the discharge performance of (Mg-Ca)-air battery by tailoring the electrolyte additives. New and earlier selected Mg^{2+} complexing agents [39, 40] are studied as potential candidates due to their ability to form soluble Mg-complexes and hinder the formation of $Mg(OH)_2$.

The effect of selected Mg^{2+} complexing agents on the corrosion behavior of Mg-Ca anode and the discharge performance of respective (Mg-Ca)-air battery is systematically investigated, which contributes to a better understanding of the working mechanism of Mg^{2+} complexing agents in aqueous Mg-air batteries.

2. Materials and methods

2.1 Materials and electrolytes

According to the research work of Deng et al. [27], with the increase of Ca content, the discharge performance of Mg-Ca becomes worse. The results of composition optimization indicate that Mg-0.1 wt. % Ca has the best discharge performance. However, the discharge performance of minor alloying Mg-Ca alloy (Ca content is less than 0.1 wt. %) has not been tested. Thus, Mg-0.04 wt. % Ca, which is denoted as Mg-Ca in the following, was prepared by the same procedure represented in the aforementioned work [27] and adopted as anode material for this work. The chemical composition of Mg-Ca alloy was analyzed via atomic absorption spectroscopy (AAS) and spark optical emission spectrometry (SOES), which is summarized in Table 1 and indicates low impurity contents (Fe, Cu and Ni).

Table 1 Chemical composition of Mg-Ca alloy (wt. %).

Materials	Ca	Mn	Si	Zn	Al	Fe	Cu	Ni	Mg
Mg-Ca	0.041	0.019	0.0086	0.0038	<0.010	0.0021	0.0012	0.0010	Bal.

The electrolyte used in this work was 3.5 wt. % NaCl solution with and without 0.1 M additives. The blank NaCl solution as background electrolyte was prepared by adopting 99% NaCl from Fisher Chemical and deionized water. The following chemicals from Sigma-Aldrich were used as electrolyte additives without further purification: citric acid (CIT); salicylic acid (SAL); 2,6-dihydroxybenzoic acid (2,6-DHB); 5-sulfosalicylic acid (5-sulfoSAL) and 3,4-dihydroxybenzoic acid (3,4-DHB). The pH of all prepared solutions was adjusted to 7.0 ± 0.3 by adding NaOH, monitored by Metrohm-691 pH meter.

2.2 Hydrogen evolution test

Hydrogen evolution tests were carried out using eudiometers. Unlike typical buret-funnel setup, eudiometer is a closed system, thus it excludes the additional intake of O_2, CO_2 and N_2 apart from

initially trapped air. The Mg-Ca samples with surface area of 15 cm^2 were tested in 500 ml solution. Before hydrogen evolution test, samples were ground up to 1200 grit emery papers and dried with cold pressed air. The immersion solution was 3.5 wt. % NaCl with and without 0.1 M electrolyte additives. During hydrogen evolution test, the electrolyte was stirred with a constant speed, 350 ± 100 rpm. The hydrogen was collected during 24 h. All tests were repeated at twice, the difference between these two tests is less than 10%.

2.3 Electrochemical measurement

Electrochemical impedance spectroscopy (EIS) measurements at OCP were performed using Gamry Reference 600 potentiostat with conventional three electrodes arrangement. Pt coiled wire worked as counter electrode, saturated Ag/AgCl electrode worked as reference electrode and Mg-Ca coupon was employed as working electrode. The surface area of working electrode was 2.5 cm^2, and before EIS measurements, Mg-Ca surface was prepared by the same procedure as the sample for hydrogen evolution test. The sample was immersed into the electrolyte for one hour prior the test to achieve stable surface state and stable open circuit potential (OCP). The tested electrode surface must be at a steady state throughout the time required for EIS measurement to ensure the accuracy of results. The applied perturbation voltage was 10 mV_{rms} and frequency range was 100 kHz - 0.01 Hz with 10.5 points per decade. All the EIS measurements were repeated three times.

2.4 Half-cell discharge test

A Gamry Interface 1000 potentiostat with typical three-electrode arrangement was used to perform the half-cell discharge tests. The sample for the half-cell test is the same as the sample for EIS test, which has the same surface area and the same preparation procedure. Half-cell discharge tests were done in a galvanostaic mode with applied current densities of 1 mA cm^{-2}, 5 mA cm^{-2}, and 10 mA cm^{-2}. Working and counter electrodes were placed in two separated beakers connected by a salt bridge (Fig. 1). The two compartments were used in order to avoid influence of rapid pH changes caused by cathodic processes on anode discharge. During discharge, the electrolyte stirred at the same speed used in hydrogen evolution test. After half-cell discharge test, the surface of the remaining Mg-Ca anode was

cleaned by aqueous solution of chromic acid to remove the discharge products and calculate the weight loss. The surface morphologies of Mg-Ca were characterized by scanning electron microscope (SEM; Tescan Vega 3) equipped with energy dispersion spectrometer (EDS; iXRF system). Utilization efficiencies of Mg-Ca alloy in different additive solutions were calculated via the following equation [41, 42]:

$$\text{Utilization efficiency (\%)} = \frac{W_{theo}}{\Delta W} \times 100\% \quad (1)$$

Where W_{theo} (g) means the theoretical weight loss of anode and ΔW (g) means the actual weight loss obtained from the mass difference of anode before and after discharge. W_{theo} was calculated via the following equation [41, 42]:

$$W_{theo} = \frac{I \times t}{F \times \sum(\frac{x_i \times n_i}{m_i})} \quad (2)$$

Where I (A) represents the applied current, t (h) represents discharge time, F is the Faraday constant (26.8 Ah mol^{-1}), x_i, n_i, m_i represent the mass fraction, ionic valence and atomic weight of the element, respectively.

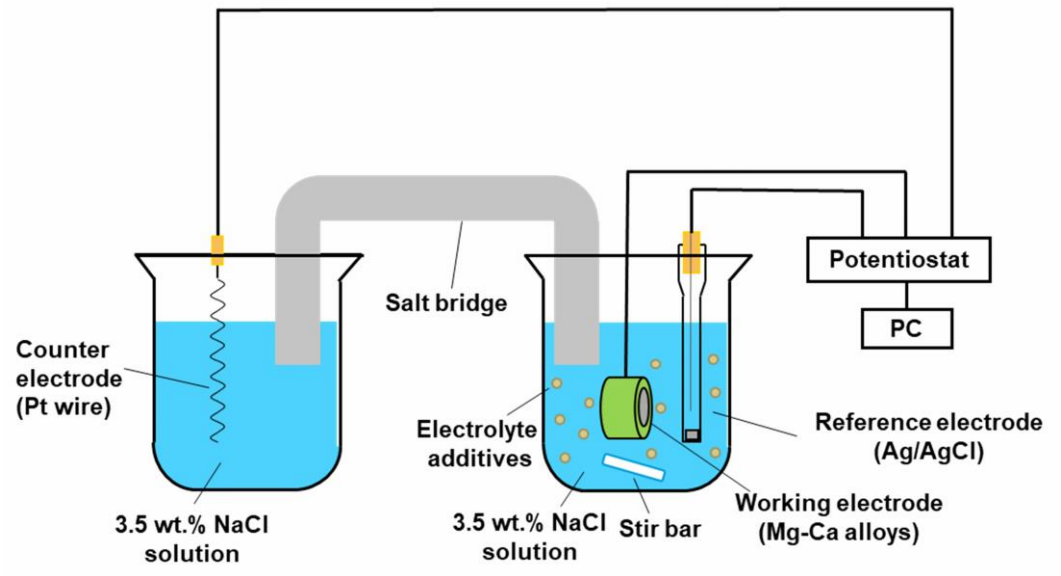

Fig. 1. Schematic of discharge test performed in half-cell arrangement.

2.5 Mg-air battery full cell test

Mg-air battery full cell tests were performed in 3.5 wt. % NaCl solution with and without additives. Mg-Ca alloy with 2.5 cm^2 surface area worked as anode and Carbon/MnO_2 fabric with PTFE gas diffusion layer and Ni mesh (Kynol Europa GmbH) worked as cathode. The discharge voltage was tested at various applied current densities 0.5 mA cm^{-2}, 1 mA cm^{-2}, 5 mA cm^{-2}, and 10 mA cm^{-2}. After discharge, the specific energy of Mg-air battery based on Mg anode was calculated via the following equation [43]:

$$\text{Specific energy (Wh kg}^{-1}) = \frac{\int_0^t I \times U \times \Delta t}{\Delta W} \quad (3)$$

Where U (V) represents the voltage of discharge, ΔW (kg) is the weight loss of anode after full cell test, I (A) and t (h) represent the same meaning as previously mentioned.

3. Results and discussion

3.1 Hydrogen evolution test

The corrosion of metallic Mg in neutral aqueous solution is accompanied by hydrogen evolution. Eq. 4 represents the global reaction of Mg corrosion, where one mole corroded Mg produces one mole hydrogen [2, 44]. Hydrogen evolution test can directly reflect the difference of the corrosion rate of Mg-Ca in different electrolytes. However, this only holds true, if oxygen reduction reaction, as secondary cathodic reaction during Mg corrosion, is negligible. Although it was recently shown that oxygen is significantly consumed at the surface of corroding Mg [45], it is still not clear what is the ratio between HER and ORR when considering cathodic process as a whole. It is assumed that the contribution of ORR to the total cathodic process is minimal in the confined volume of eudiometers used in current work.

$$Mg + 2H_2O \rightarrow Mg(OH)_2 + H_2\uparrow \quad (4)$$

Fig. 2a represents the volume of evolved hydrogen during 24 hours test. Several additives with different abilities to form complexes with Mg^{2+} were tested. The lowest hydrogen volume, thus the lowest corrosion rate, was detected for Mg-Ca in blank 3.5 wt. % NaCl solution, which demonstrates

good corrosion resistance. All selected additives accelerated the dissolution of Mg-Ca in NaCl solution at different extent. The different hydrogen evolution rate can be correlated to the stability constants of Mg^{2+} complexes, which are listed in Table 2 except for 2,6-DHB. The information about stability constant of complexes formed by 2,6-DHB with Mg^{2+} was not found in literature. It should be noted that the main idea behind choice of additives was their ability to keep anode surface clean during discharge, namely, their ability to produce soluble complexes with Mg^{2+} of mild stability. Hence, the generation of $Mg(OH)_2$ is retarded and the IR drop caused by $Mg(OH)_2$ is diminished during discharge. However, it might also increase the corrosion rate of Mg-Ca without load or with low current load, especially if an additive forms highly stable complexes with Mg^{2+} and the stability constant is high.

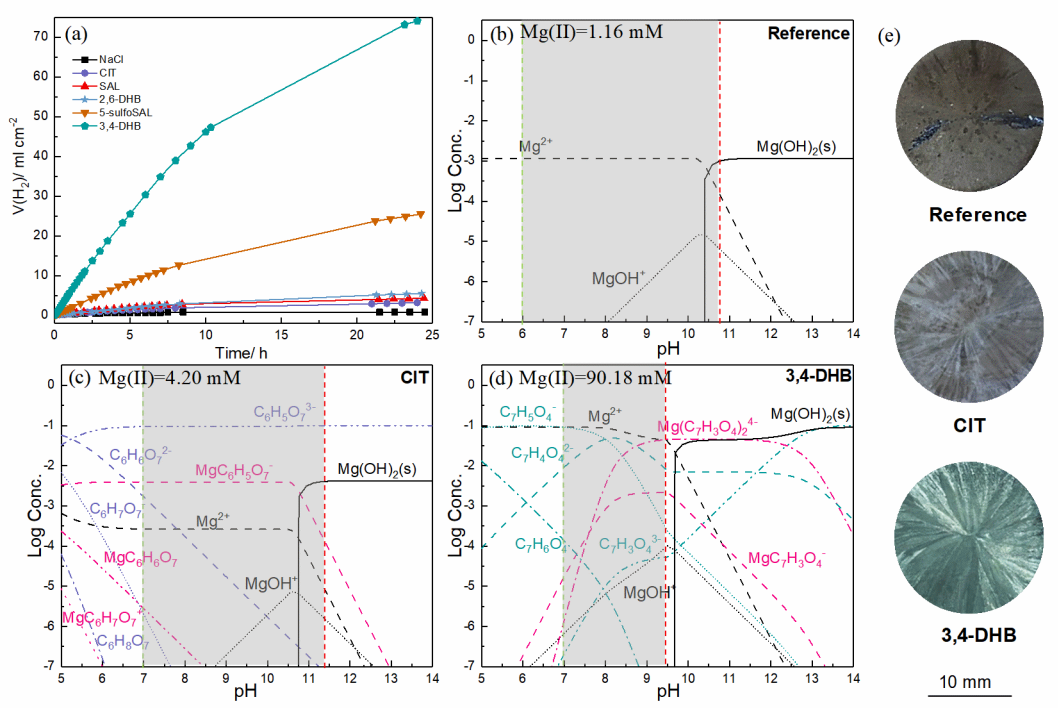

Fig. 2. (a) Hydrogen evolution curve of Mg-Ca in 3.5 wt. % NaCl solution with and without additives and thermodynamic calculation of the equilibrium composition of relevant species in (b) blank 3.5 wt. % NaCl; and the same electrolyte with 0.1 M (c) CIT; and (d) 3,4-DHB. The green and red lines present the initial pH and the final pH after 24h hydrogen evolution test. The optical images of samples after 24 hours hydrogen evolution test are shown in (e).

Hydra-Medusa software was adopted here to simulate the possible chemical equilibria in order to estimate the in-situ surface condition of Mg-Ca alloy after 24 h hydrogen evolution test in the presence

and absence of selected additives. The estimated concentration of Mg(II) ions in different additive solution was calculated from the result of hydrogen evolution test: 1.16 mM for blank NaCl solution, 4.20 mM for NaCl solution with 0.1 M CIT and 90.18 mM for NaCl solution with 0.1 M 3,4-DHB. The difference in the initial concentration of Mg(II) ions will influence the critical pH for the generation of $Mg(OH)_2$, namely, the generation of precipitates. The results of Hydra-Medusa simulation are plotted in Fig. 2.

Fig. 2b shows the formation of insoluble $Mg(OH)_2$ in blank NaCl solution takes place at pH 10.4. The final pH of blank NaCl solution after 24 h hydrogen evolution test is 10.7, which is above 10.4, and insoluble corrosion products start to precipitate on Mg-Ca alloy surface at this pH, like Fig. 2e shows. When 0.1 M CIT as Mg^{2+} complexing agent is introduced to NaCl solution (Fig. 2c), the precipitation of $Mg(OH)_2$ is delayed from pH 10.4 to pH 10.8 even the total amount of Mg(II) ions generated by the dissolution of Mg-Ca is higher than in blank NaCl solution. From Fig. 2c, soluble Mg-ligand complexes form and exist in a wide pH range at least from pH 5 to 14. Hence, even the total amount of Mg(II) ions is higher, the free Mg^{2+} in the solution is even less than in blank NaCl solution. Between the pH ranges from 7 to 10.8, soluble complexes form and the dissolution of Mg-Ca is accelerated. However, after 24 h hydrogen evolution test, the final pH of this solution is 11.4, which exceeds the critical pH. The formed precipitates changed the color of Mg-Ca alloy surface, as shown in Fig. 2e. According to Fig. 2a, a large amount of Mg-Ca was dissolved into NaCl solution with 0.1 M 3,4-DHB. Thus, the total amount of Mg(II) ions in NaCl solution with 0.1M 3,4-DHB is almost hundred times higher than that for blank NaCl solution. Even 3,4-DHB possesses the strongest complexation ability among selected additives, the concentration of free Mg^{2+} in NaCl solution with 0.1 M 3,4-DHB is still higher than that in blank NaCl solution (Fig. 2d). Hence, the critical pH in NaCl solution with 0.1 M 3,4-DHB is 9.7, which is lower than the critical pH in blank NaCl solution. As Fig. 2d shows, Mg complexes with 3,4-DHB ($Mg(C_7H_3O_4)_2^{4-}$ and $MgC_7H_3O_4^-$) exist and are stable at high pH, especially for $Mg(C_7H_3O_4)_2^{4-}$. After 24 h hydrogen evolution test, the final pH of NaCl solution with 3,4-DHB is 9.5, which does not exceed the critical pH for the generation of stable precipitates. This is in line with the experimentally observed surface of Mg-Ca alloy in NaCl solution with 3,4-DHB, which is macroscopically clean with metallic luster and without the coverage of $Mg(OH)_2$ (Fig. 2e). When 3,4-

DHB is adopted as electrolyte additives for Mg-air battery, it might hinder the precipitation of discharge products and increase the anode activity during discharge.

Table 2 Stability constants of Mg^{2+} complexes produced by selected electrolyte additives and equilibrium constants of selected additives after 24 hours hydrogen evolution tests [46-48].

Complexing agent	Stability constants		pH after 24 h of hydrogen evolution test (initial pH 7)
	$logKMg^{2+}$	Ref.	
NaCl reference	-	-	10.7
CIT	ML/M.L 3.45 MHL/M.HL 1.81 MH2L/M. H2L 0.7	[48]	11.4
SAL	ML/M.L 4.7	[46]	11.2
2,6-DHB	n/a	-	11.2
5-sulfoSAL	ML/M.L 5.1 MHL/M.HL 0.73	[48]	11.0
3,4-DHB	ML/M.L 5.67 ML2/M.L2 9.84	[47]	9.5

As Table 2 shows, the final pH of tested electrolyte containing CIT, SAL, 5-sulfoSAL and 2,6-DHB is higher than the final pH of blank NaCl solution, because OH^- generated during hydrogen evolution reaction(HER, Eq. 4) is barely consumed for formation of $Mg(OH)_2$. However, the final pH of NaCl solution with 3,4-DHB is lower than 10.7. 3,4-DHB has the strongest complexation ability with Mg^{2+} among selected additives and the amount of hydrogen evolved within 24 hours test is the highest. Therefore, the amount of OH^- released into the electrolyte should be even higher than in other additive solutions. From Table 2 and Fig. 2d, the bulk pH of NaCl solution with 3,4-DHB increased to 9.5 after 24 h hydrogen evolution test and the complexation reaction between Mg^{2+} and 3,4-DHB can be written as Eq. 5 and Eq. 6 [49, 50].

$$Mg^{2+} + (C_7H_5O_4)^- \rightarrow MgC_7H_3O_4^- + 2H^+ \quad (5)$$

$$MgC_7H_3O_4^- + (C_7H_5O_4)^- \rightarrow Mg(C_7H_3O_4)_2^{4-} + 2H^+ \quad (6)$$

Most of the OH^- generated during HER (Eq. 4) is consumed to neutralize the H^+ generated by complexation reaction (Eq. 5 and Eq. 6). Therefore, the final pH of electrolyte containing 3,4-DHB is the lowest and the formation of $Mg(OH)_2$ in this electrolyte is more difficult than in other electrolytes.

3.2 Impedance measurement

The effect of selected additives on the self-corrosion behavior of Mg-Ca was also determined by electrochemical impedance spectroscopy (EIS). The Nyquist plot of Mg-Ca anode in different electrolytes (Fig. 3a and 3b) revealed two capacitive loops. The high frequency one relates to the natural oxide layer presented on the surface of Mg-Ca and the middle frequency one relates to the charge transfer process [27, 51]. In presence of additives, two capacitive loops at high and middle frequencies were followed by a low frequency inductive loop. The origin of the inductive loop presented on EIS spectra of Mg alloys is generally subject of discussion. It has been attributed to non-stationarity during measurements [52, 53]. The origin of the inductive like behavior at low frequencies requires detailed investigation, which is out of the scope of this work.

In order to quantitatively evaluate the effect of additives on the behavior of Mg-Ca alloy, the EIS spectra were fitted with the equivalent circuit shown in Fig. 3c. The inductive loop was not considered in fitting process, hence the EIS results were fitted to different low frequency limits, like 0.02 Hz for NaCl and 0.2 Hz for 5-sulfoSAL. In this circuit, R_s means the internal resistance of the electrolyte. R_f and CPE_f are the resistance and capacitance of the oxide film respectively. R_{ct} represents the resistance due to charge transfer and CPE_{dl} is the electric double layer capacitance. The fitting results are presented in Fig. 3d. With the presence of additives in 3.5 wt. % NaCl solution, both the R_f and the R_{ct} decreased in the following order: 3.5 wt. % NaCl > CIT > SAL > 2,6-DHB > 5-sulfoSAL > 3,4-DHB. This order directly corresponds to the ranking of the additives during the hydrogen evolution test. In blank NaCl solution, Mg-Ca alloys released the least amount of H_2 while in presence of 3,4-DHB the amount of released H_2 was the highest. It is noticed that, with the addition of 5-sulfoSAL and 3,4-DHB, the

calculated values of R_f and R_{ct} were much lower than the R_f and R_{ct} in blank 3.5 wt. % NaCl solution, as presented in Fig. 3d. In the electrolytes with these two kinds of additives, the dissolution rates of Mg-Ca were much faster than in other electrolytes. Low R_{ct} indicates the low corrosion resistance and high dissolution rate. It is apparent that the presence of additives increased the dissolution rate. Low R_{ct} also reflects better discharge activity of Mg-Ca in electrolyte with selected additives. Notably, the presence of additives decreased the overall impedance. This is probably due to their ability to form soluble complexes with Mg^{2+}, which stimulates the dissolution kinetic via near surface interaction. A correlation show: the higher is stability constant of the involved complex the faster Mg gets dissolved. These results are in a good agreement with the hydrogen evolution tests.

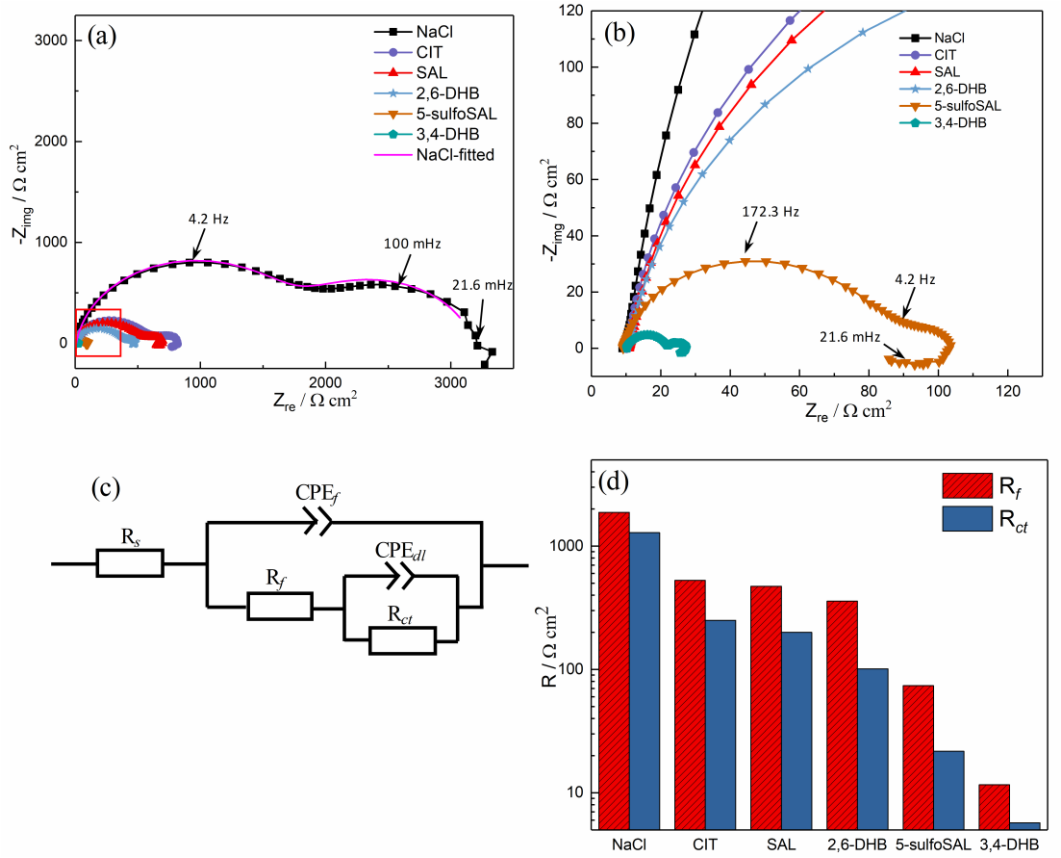

Fig. 3. EIS results of Mg-Ca in 3.5 wt. % NaCl solution with and without different additives: (a) Nyquist plots; (b) and magnification of the high frequency part of (a); (c) Equivalent circuit; (d) Film resistance and charge transfer resistance (log scale).

3.3 OCP and Half-cell discharge test

Fig. 4 indicates the half-cell discharge performance of Mg-Ca alloys in presence of different electrolyte additives. Once the selected substances were added to the blank NaCl solution, the OCP of Mg-Ca decreased (Fig. 4a). The OCP of the anode in presence of 5-sulfoSAL reached -1.98 V (vs Ag/AgCl), which was 200 mV lower than that in blank NaCl solution. During one hour test, the OCP of Mg-Ca in 3,4-DHB kept changing because the reaction on anode surface was too intense to achieve the stable state. Mg-Ca at 1 mA cm^{-2} revealed more negative discharge potential with 2,6-DHB, 3,4-DHB and 5-sulfoSAL additives in comparison with blank NaCl. The discharge potential of Mg-Ca in CIT and SAL solution was also more negative than the reference. Whereas the discharge current density is 5 mA cm^{-2}, the discharge potential of Mg-Ca became more positive with less or no differences in potential between blank NaCl and NaCl solution with CIT. In NaCl solution with SAL, the initial discharge potential of Mg-Ca was more negative than that in the blank NaCl solution. However, after 14 hours, the discharge potential of Mg-Ca in NaCl solution with SAL increased sharply and the final discharge potential was even higher than the reference. Strong Mg^{2+} complexing agents, like 5-sulfoSAL and 3,4-DHB, maintained a relatively negative discharge potential with a decreasing tendency even after 24 hours discharge. The discharge potential of Mg-Ca with 2,6-DHB was 50 mV lower than the reference and relatively stable along 24 hours test. At 10 mA cm^{-2}, the discharge potential of Mg-Ca in NaCl solution with SAL increased rapidly to positive direction after 4 hours discharge. In NaCl solution with CIT, the discharge potential of Mg-Ca was also more positive than in blank NaCl solution. Nevertheless, with the addition of 5-sulfoSAL, 2,6-DHB and 3,4-DHB the discharge potential of the anode was still more negative than the reference.

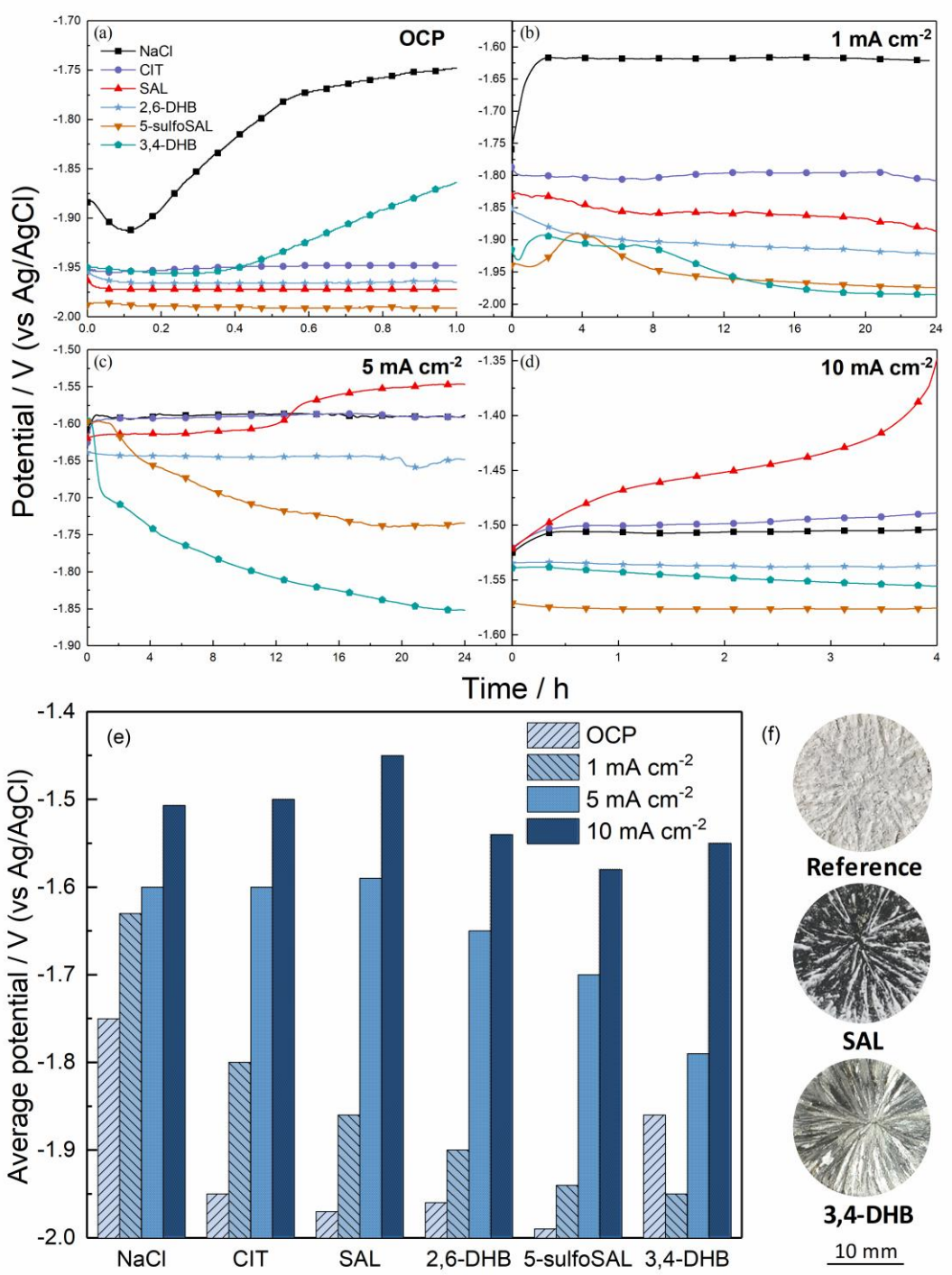

Fig. 4. Discharge curves of Mg-Ca in 3.5 wt. % NaCl solution with and without different additives at current density: (a) open circuit; (b) 1; (c) 5; (d) 10 mA cm^{-2}; (e) average discharge potential of Mg-Ca at different current densities; and (f) macro-morphologies of Mg-Ca after 24 hours discharge test at 5 mA cm^{-2} in different electrolytes.

The discharge potential of anodes in half-cell can be expressed as:

$$E_{anode} = E_{ocp} - \eta_{ct} - \eta_{diff} - IR \quad (7)$$

Where E_{ocp} represents the open circuit potential, $\boldsymbol{\eta}_{ct}$ means the potential drop related to charge transfer process, $\boldsymbol{\eta}_{diff}$ is the potential drop due to discharge products (e.g. transport aspect), I and R represents the applied current and the resistance of electrolyte between metal surface of working anode and the reference electrode [1, 27, 54]. According to this equation, the improvement of discharge potential of an anode can be achieved by more negative open circuit potential and minimization of potential drop caused by discharge products. The average value of open circuit potential of Mg-Ca in different electrolytes in the last 10 minutes of the test is presented in Fig. 4e, because the open circuit potential of Mg-Ca in the last 10 minutes is more stable than at the beginning of the test. The average discharge potentials of Mg-Ca at different current densities during 24 h discharge are also calculated and presented in Fig. 4e. Obviously, all selected electrolyte additives led to more negative OCP values of the tested anode material. As shown in Fig. 4e, all electrolyte additives efficiently made the average discharge potential of Mg-Ca anode more negative when the applied current density was 1 mA cm^{-2}. At 5 and 10 mA cm^{-2}, the average discharge potential of Mg-Ca in electrolyte containing moderate additives, like CIT and SAL, was similar to that in blank NaCl solution. In electrolyte containing 2,6-DHB, 5-sulfoSAL and 3,4-DHB, the average discharge potential of Mg-Ca was always more negative than the average discharge potential of Mg-Ca in blank NaCl solution. As the optical images in Fig. 4f show, the surface of Mg-Ca in blank NaCl solution was fully covered by discharge products after half-cell discharge test. With the presence of moderate additive SAL, the deposition of discharge products was not inhibited, while in electrolyte containing 3,4-DHB, the surface was clean and without any discharge products.

The deposition of discharge products was further evaluated by SEM of the samples after discharge test. Fig. 5 presents the surface morphology of Mg-Ca after 24h discharge in blank NaCl solution, in NaCl solution with SAL and in NaCl solution with 3,4-DHB at dry condition. The surface of Mg-Ca in blank NaCl solution was completely covered by discharge products. At 1 mA cm^{-2} (Fig. 5a), the layer was thick with some big cracks. After discharged at higher current density, the discharge products

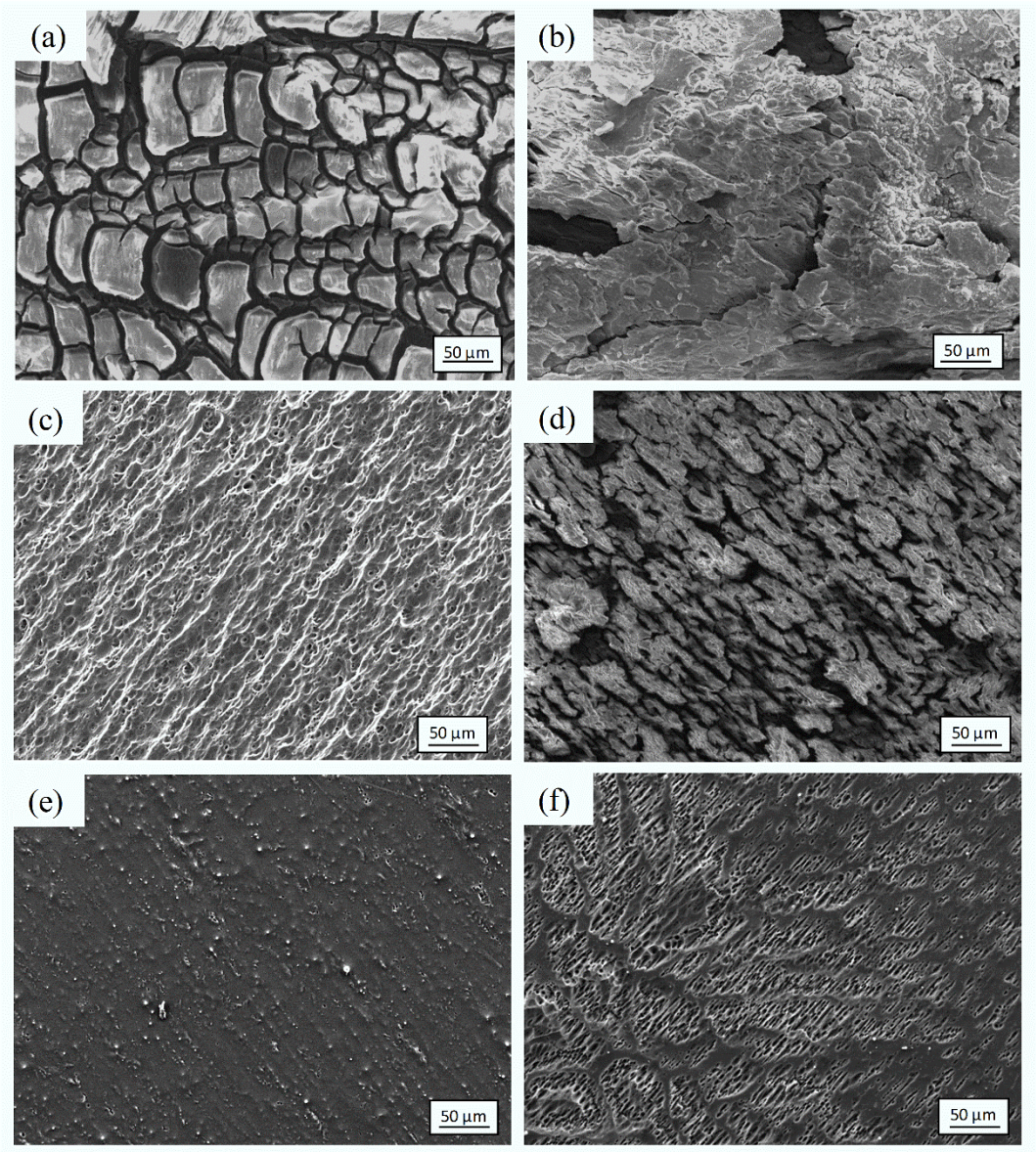

Fig. 5. Surface morphologies of Mg-Ca after 24 hours discharge in 3.5 wt. % NaCl (a) without additive at 1 and (b) 5 mA cm^{-2}; (c) with SAL at 1 and (d) 5 mA cm^{-2}; (e) with 3,4-DHB at 1 and (f) 5 mA cm^{-2} measured via SEM on dried but uncleaned anode.

became denser without large cracks (Fig. 5b). In presence of SAL, at 1 mA cm^{-2}, the anode surface was clean without discharge products. However, discharge products fully covered the anode surface at 5 mA cm^{-2}. In presence of 3,4-DHB, which has the strongest ability to form soluble complex with Mg^{2+}, the formation of discharge products film was not observed at both current densities. From the surface morphologies of Mg-Ca anode after discharge (Fig. 5), it is possible to conclude that selected electrolyte additives retarded the formation of discharge products to different degrees, contributing to less overpotential during discharge test at small current density. For discharge tests at large current density,

the dissolution of anode material is faster. The electrolyte additives should have stronger complexation ability and faster kinetics to hinder the formation of discharge products. For SAL and CIT, which have relatively weak complexation ability with Mg^{2+}, both of them could not prevent the formation of discharge products at 5 and 10 mA cm^{-2}. Hence, the discharge potential of the anode in these two additive solutions either shows no apparent difference to the reference test or becomes even more positive than the reference test. 3,4-DHB decreases the OCP of Mg-Ca as it possesses the strongest ability to form soluble complex with Mg^{2+}, which means the overpotential caused by discharge products is the lowest. Hence, the average discharge potentials of the anode in NaCl solution with 3,4-DHB were always 40-320 mV more negative than that in blank NaCl solution.

3.4 Utilization efficiency

Utilization efficiency of an anode is an essential technical factor to be considered when evaluating the discharge performance of anode materials in different electrolytes. The utilization efficiencies of Mg-Ca in different electrolytes are presented in Table. 3. In comparison with Mg-Al-Zn, Mg-Al-Pb, Mg-Al-In, Mg-Al-Sn [12, 17, 30, 55-57], Mg-Ca alloy with low Ca content shows relatively high utilization efficiency when acts as anode material, 58.2% and 55.6%, respectively at 5 and 10 mA cm^{-2} [27]. Nevertheless, the utilization efficiency of Mg-Ca can be additionally improved by adopting electrolyte additives. The influence of selected electrolyte additives on the utilization efficiency of Mg-Ca depends on the complexation ability and applied current density as listed in the Table. 3. At 1 mA cm^{-2}, Mg-Ca showed highest utilization efficiency in NaCl solution with CIT. It reached 64.7%, 12% higher than the utilization efficiency of Mg-Ca in blank NaCl solution. The addition of other complexing agents at the same applied current density decreased the utilization efficiency of Mg-Ca due to the fast consumption of anode supported by complexing of Mg^{2+}. At 5 mA cm^{-2}, the Mg-Ca in blank NaCl solution revealed 60.0% utilization efficiency. With the addition of 2,6-DHB and SAL, the utilization efficiencies were further improved to 65.0% and 62.9% respectively. The highest utilization efficiency 67.2% at 10 mA cm^{-2} was achieved for 2,6-DHB. In the case of 5-sulfoSAL and 3,4- DHB, which have strong ability to form complex with Mg^{2+}, the utilization efficiencies of Mg-Ca increased

with the increase of current density. In these two additive solutions, the utilization efficiencies of Mg-Ca at 10 mA cm^{-2} reached 61.7% and 62.3%, respectively.

Table 3 Utilization efficiency (in %) of Mg-Ca in 3.5 wt. % NaCl solution with and without different electrolyte additives at current densities 1, 5 and 10 mA cm^{-2}.

Current density	3.5 wt. % NaCl	CIT	SAL	2,6-DHB	5-sulfoSAL	3,4-DHB
1 mA cm^{-2}	53.0 ± 0.1	64.7 ± 2.7	46.3 ± 4.5	37.8 ± 0.5	24.6 ± 5.2	9.0 ± 0.6
5 mA cm^{-2}	60.0 ± 2.2	60.5 ± 2.8	62.9 ± 2.2	65.0 ± 1.5	56.1 ± 1.4	35.6 ± 2.1
10 mA cm^{-2}	59.7 ± 3.2	56.5 ± 1.0	58.8 ± 3.8	67.2 ± 0.7	61.7 ± 3.5	62.3 ± 0.2

According to Eq. 1, utilization efficiency shows the difference between the actual weight loss and the calculated theoretical value. The actual weight loss consists of the theoretical weight loss, the weight loss due to self-corrosion and the weight loss due to chunk effect [20, 58, 59]. The chunk effect specifically refers to the weight loss caused by the detachment of metallic particles from the anode surface [60, 61]. The theoretical weight loss of anode material follows Faraday's law. The difference of utilization efficiency of Mg-Ca in general in presence of different additives is caused by the various contribution from self-corrosion and the chunk effect. As shown in Fig. 2a, Mg-Ca had a very low hydrogen evolution rate in blank NaCl solution, therefore high corrosion resistance. With the addition of selected Mg^{2+} complexing agents, the corrosion resistance decreased due to faster Mg dissolution. However, as shown in Table 3, the highest utilization efficiency was achieved by adding different Mg^{2+} complexing agents. One of the reasons could be the ability of all selected additives to decrease the chunk effect. Fig. 6 presents the SEM (BSE) images of the cross section of Mg-Ca after 24 hours discharge tests at 5 mA cm^{-2} in different electrolytes. The anode suffered from chunk effect in blank NaCl solution. As shown in Fig. 6a, the surface of tested Mg-Ca was covered by discharge products. In several locations, undissolved Mg-Ca matrix was completely surrounded by discharge products and lost contact with the bulk anode matrix (Fig. 6a) and did not contribute to the measured electric current. Besides, inside the bulk anode matrix, some (tortuous) channels were formed during discharge. This may cause the metal spalling and formation of undissolved metallic chunks. During discharge, those undissolved metallic chunks were trapped by discharge products or released into the electrolyte. This

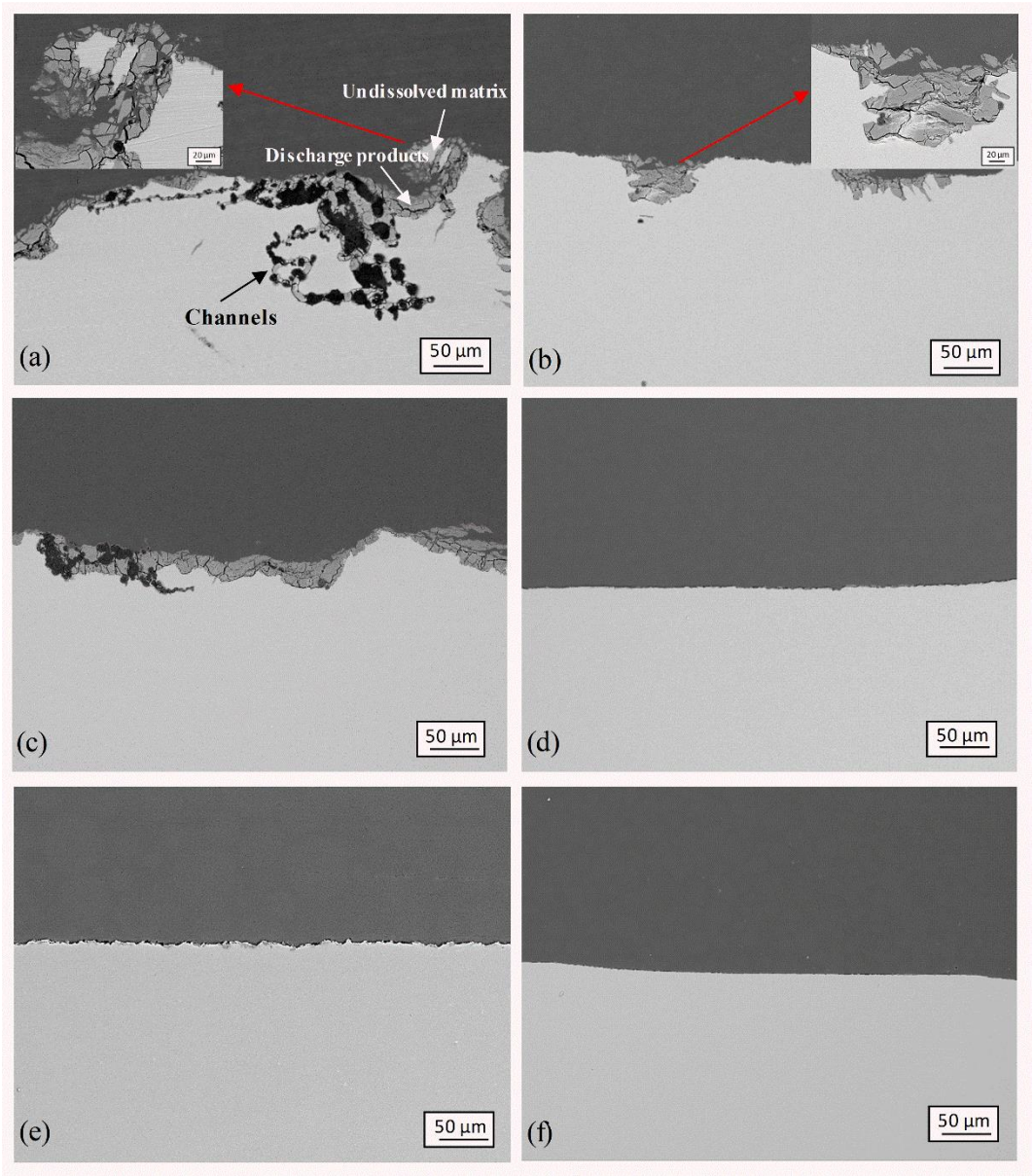

Fig. 6. Cross-section SEM images(BSE mode) of Mg-Ca after 24 hours discharge at 5 mA cm^{-2} in (a) 3.5 wt. % NaCl and the same electrolyte with 0.1M (b) CIT; (c) SAL; (d) 5-sulfoSAL; (e) 2,6-DHB; (f) 3,4-DHB.

leads to weight loss of anode without any contribution to the discharge current. In turn, this massively causes the decrease of utilization efficiency [60, 62]. As shown in Fig. 6b, only part of the Mg-Ca surface accumulated discharge products and only few metallic particles were entrapped by discharge products. Moreover, except for in NaCl solution with CIT, no apparent chunk effect was found in NaCl solution with other selected additives. In NaCl solution with SAL, the thin layer of corrosion producs was formed on the surface of the anode but entrapped metallic particles were not detected (Fig. 6c). In NaCl solution with 5-sulfoSAL, 2,6-DHB and 3,4-DHB, Mg-Ca anode surfaces were completely clean

with no evidence of chunk effect. The weight loss caused by chunk effect in these three additive solutions was negligible. According to Fig. 2a, among these additives, Mg-Ca shows the lowest corrosion rate in NaCl solution with 2,6-DHB, which exhibits the moderate Mg^{2+} complexation ability. Thus, 2,6-DHB would not greatly additionally dissolve anode material during discharge comparing to 5-sulfoSAL and 3,4-DHB. Therefore, Mg-Ca in NaCl solution with 2,6-DHB shows the highest utilization efficiency at 5 mA cm^{-2}.

3.5 Mg-air full battery discharge test

In order to clarify the effect of selected electrolyte additives on the discharge performance of aqueous (Mg-Ca)-air battery, full-cell discharge tests were done in a lab-made Mg-air battery setup. The discharge curves of (Mg-Ca)-air batteries in various electrolytes at defined current densities are presented in Fig. 7. All the selected additives greatly increased the output voltage of the cell. In NaCl solution with 5-sulfoSAL, (Mg-Ca)-air battery exhibited the highest and quite stable discharge voltage at 0.5 and 1 mA cm^{-2}, which is ~ 1.86 and 1.82 V, respectively, compared to ~ 1.60 and 1.55 V in the blank NaCl solution. At 5 mA cm^{-2}, the addition of Mg^{2+} complexing agents kept the battery voltage higher than that of Mg-air battery in blank NaCl solution. The highest voltage value, ~ 1.58 V, was obtained in NaCl solution with 3,4-DHB. As the applied current density was 10 mA cm^{-2}, SAL and CIT additives could not efficiently hinder the formation of discharge products, and therefore, the Mg-air batteries failed. However, in NaCl solution with 2,6-DHB, 3,4-DHB and 5-sulfoSAL, which have relatively high complexation ability with Mg^{2+}, the battery voltages were still enhanced, by 70-110 mV, compared to the reference.

The specific energy of (Mg-Ca)-air batteries in different electrolytes at various current densities is shown in Fig. 8. At lower discharge currents, higher specific energy was achieved by adding CIT and SAL. Both of them have relatively weak complexation ability with Mg^{2+}. The lower current density indicates lower rate of Mg^{2+} produced by discharge process. Those complexing agents with mild complexation ability can retard the formation of discharge product film and maintain high discharge voltage without additional dissolution of Mg based anode. Hence, the highest specific energy was

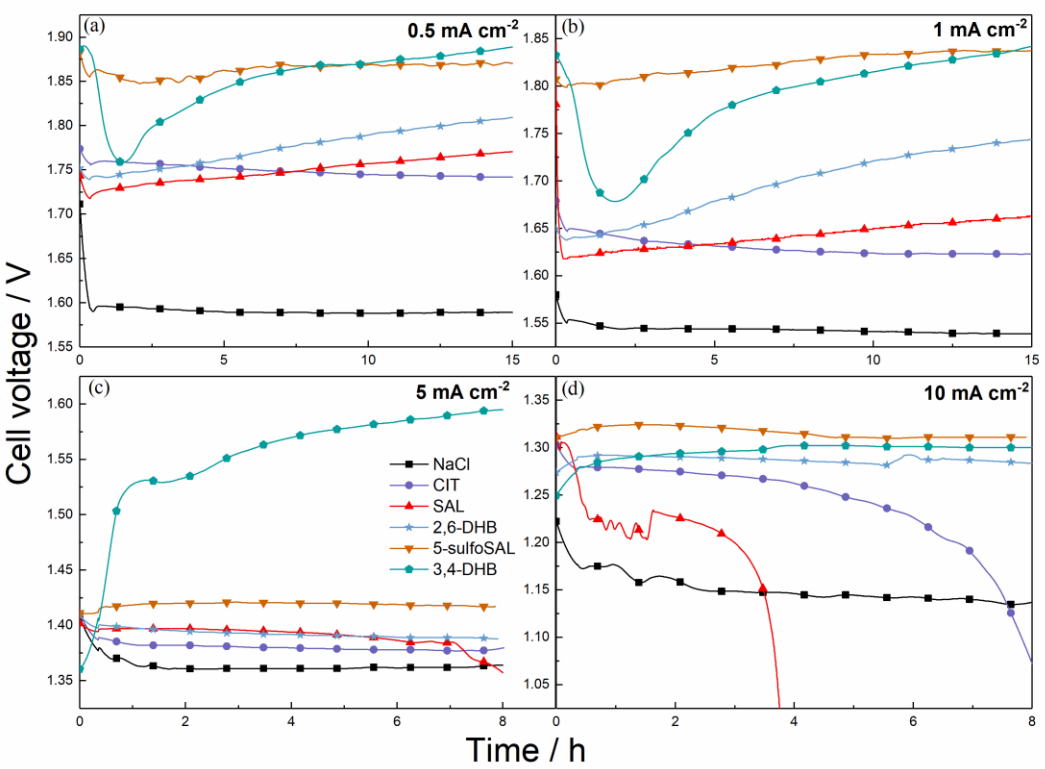

Fig. 7. Discharge performance of (Mg-Ca)-air battery in 3.5 wt. % NaCl solution with and without additives at various current densities: (a) 0.5; (b) 1; (c) 5 and (d) 10 mA cm^{-2}.

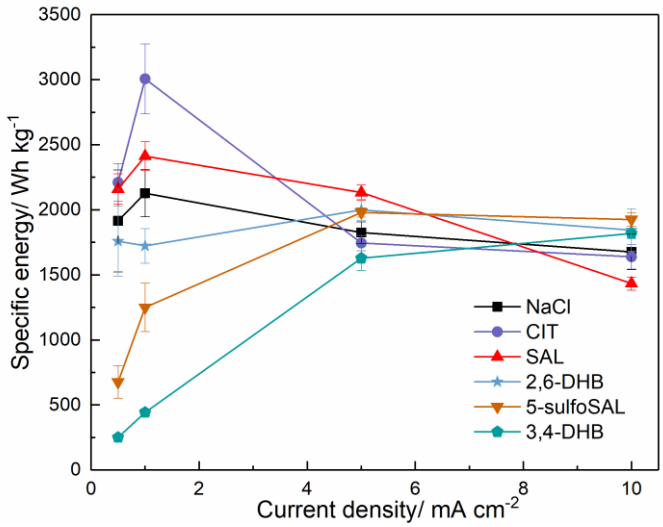

Fig. 8. Specific energy of (Mg-Ca)-air battery in 3.5 wt. % NaCl solution with and without additives at various current densities.

achieved by adding CIT at 1 mA cm^{-2}. It reached 3007 Wh kg^{-1}, which was 880 Wh kg^{-1} higher than the specific energy of (Mg-Ca)-air battery in blank NaCl solution at 1 mA cm^{-2}. Compared with literatures [13, 27, 36, 63-65], it is much higher than the specific energy of Mg-air battery based on different Mg alloys anodes in different aqueous electrolytes, although the different experimental environment and

cathode materials might cause deviations. The specific energy of (Mg-Ca)-air battery in moderate additive solution decreased with the increase of current density. At relatively high current density, a higher rate of Mg^{2+} generated and released into the electrolyte. In this case complexing agents with strong ability of forming complex with Mg^{2+}, like 2,6-DHB, 3,4-DHB and 5-sulfoSAL, keep the anode surface clean, maintaining a relatively high cell voltage. At the same time, they do not greatly dissolve the additional anode materials because a large amount of Mg^{2+} exists in the electrolyte. Therefore, (Mg-Ca)-air batteries containing 2,6-DHB, 3,4-DHB and 5-sulfoSAL had relatively high specific energy at 10 mA cm^{-2}. The effect of selected electrolyte additives depends on the applied current density and the complexation ability with Mg^{2+}.

4. Conclusions

In this work, Mg^{2+} complexing agents were used as electrolyte additives for aqueous Mg-air battery. The effect of the electrolyte additives on the corrosion behavior and discharge performance of Mg-Ca was investigated.

(1) Additives that form soluble complexes with Mg^{2+} overall have positive effect on the discharge performance of (Mg-Ca)-air battery. According to their complexation ability with Mg^{2+}, different additives should be used for different discharge loads to obtain optimal effect.

(2) Stability constants of soluble complexes with Mg^{2+} is an important aspect enhancing anode activity. (Mg-Ca)-air battery at lower discharge current exhibits ideal performance by using additives with moderate stability constant, such as CIT and SAL. At higher discharge loads, better performance is achieved when using the additives with strong complexation ability, such as 3,4-DHB and 5-sulfoSAL. The peak specific energy appears at 1 mA cm^{-2} in NaCl with CIT and reaches 3007 Wh kg^{-1}. At 10 mA cm^{-2}, the specific energy of Mg-Ca in NaCl solution with 5-sulfoSAL is the highest, achieving 1925 Wh kg^{-1}.

(3) The selected additives hinder the formation of discharge products on the anode surface and provide more active area for discharge according to their different complexation ability with Mg^{2+}, resulting in more negative OCP and less potential drop caused by discharge products. In

half-cell discharge test, the average discharge potential of Mg-Ca in NaCl with 0.1M 3,4-DHB reaches -1.95 V at 1 mA cm^{-2}, which is 320 mV more negative than that in blank NaCl solution. In full-cell discharge test, the highest cell voltage of (Mg-Ca)-air battery is achieved by the usage of 5-sulfoSAL at 0.5 mA cm^{-2}, 1.86 V, which is 270 mV higher than the reference.

(4) At low current density, the addition of strong complexing agent (like 3,4-DHB) causes significant loss of utilization efficiency. However, the utilization efficiency of Mg-Ca is improved by using moderate Mg^{2+} complexing agents at relatively high current density. The highest utilization efficiency was shown for 2,6-DHB (65% at 5 mA cm^{-2} and 67.2% at 10 mA cm^{-2}), because the addition of 2,6-DHB makes the dissolution of Mg-Ca more uniform, eliminating the weight loss caused by chunk effect which is significant in pure NaCl solution.

Acknowledgements

The authors would like to acknowledge the technical support from Mr. Ulrich Burmester, Mr. Volker Heitmann and Mr. Gert Wiese. L. Wang and M. Deng are grateful for the award of fellowship from China Scholarship Council (No. 201706370183 and No. 201606370031). Dr. D. Snihirova would like to acknowledge Alexander von Humboldt foundation for financial support via postdoctoral grant. Additionally, the authors acknowledge SeaMag project funded by ERA-NET cofund MarTERA.

References

[1] D. Linden, T.B. Reddy, Handbook of Batteries, McGraw-Hill, New York, 2002.
[2] T. Zhang, Z. Tao, J. Chen, Mater. Horiz., 1 (2014) 196-206. http://doi.org/10.1039/c3mh00059a.
[3] M. Fichtner, B.J. Ingram, E. Sheridan, R. Mohtadi, C. Battaglia, Z. Zhao-Karger, P. Canepa, R. Dominko, D. Hoeche, M. Weil, Magnesium Batteries: Research and Applications, Royal Society of Chemistry, 2019.
[4] F. Cheng, J. Chen, Chem Soc Rev, 41 (2012) 2172-2192. http://doi.org/10.1039/c1cs15228a.
[5] D. Cao, L. Wu, Y. Sun, G. Wang, Y. Lv, Journal of Power Sources, 177 (2008) 624-630. http://doi.org/10.1016/j.jpowsour.2007.11.037.
[6] R. Mohtadi, F. Mizuno, Beilstein J Nanotechnol, 5 (2014) 1291-1311. http://doi.org/10.3762/bjnano.5.143.
[7] H.D. Yoo, I. Shterenberg, Y. Gofer, G. Gershinsky, N. Pour, D. Aurbach, Energy & Environmental Science, 6 (2013) 2265. http://doi.org/10.1039/c3ee40871j.
[8] M. Esmaily, J.E. Svensson, S. Fajardo, N. Birbilis, G.S. Frankel, S. Virtanen, R. Arrabal, S. Thomas, L.G. Johansson, Progress in Materials Science, 89 (2017) 92-193. http://doi.org/10.1016/j.pmatsci.2017.04.011.

[9] S. Fajardo, G.S. Frankel, Electrochimica Acta, 165 (2015) 255-267. http://doi.org/10.1016/j.electacta.2015.03.021.
[10] M. Yuasa, X. Huang, K. Suzuki, M. Mabuchi, Y. Chino, Journal of Power Sources, 297 (2015) 449-456. http://doi.org/10.1016/j.jpowsour.2015.08.042.
[11] L. Wen, K. Yu, H. Xiong, Y. Dai, S. Yang, X. Qiao, F. Teng, S. Fan, Electrochimica Acta, 194 (2016) 40-51. http://doi.org/10.1016/j.electacta.2016.02.088.
[12] H. Xiong, K. Yu, X. Yin, Y. Dai, Y. Yan, H. Zhu, Journal of Alloys and Compounds, 708 (2017) 652-661. http://doi.org/10.1016/j.jallcom.2016.12.172.
[13] X. Liu, J. Xue, P. Zhang, Z. Wang, Journal of Power Sources, 414 (2019) 174-182. http://doi.org/10.1016/j.jpowsour.2018.12.092
[14] T. Zheng, Y. Hu, Y. Zhang, S. Yang, F. Pan, Materials & Design, 137 (2018) 245-255. http://doi.org/10.1016/j.matdes.2017.10.031.
[15] Y. Feng, R. Wang, K. Yu, C. Peng, J. Zhang, C. Zhang, Journal of Alloys and Compounds, 473 (2009) 215-219. http://doi.org/10.1016/j.jallcom.2008.05.054.
[16] N. Wang, R. Wang, Y. Feng, W. Xiong, J. Zhang, M. Deng, Corrosion Science, 112 (2016) 13-24. http://doi.org/10.1016/j.corsci.2016.07.002.
[17] N. Wang, R. Wang, C. Peng, B. Peng, Y. Feng, C. Hu, Electrochimica Acta, 149 (2014) 193-205. http://doi.org/10.1016/j.electacta.2014.10.053.
[18] G. Huang, Y. Zhao, Y. Wang, H. Zhang, F. Pan, Materials Letters, 113 (2013) 46-49. http://doi.org/10.1016/j.matlet.2013.09.041.
[19] Y. Lv, Y. Xu, D. Cao, Journal of Power Sources, 196 (2011) 8809-8814. http://doi.org/10.1016/j.jpowsour.2011.06.001.
[20] L. Wang, R. Wang, Y. Feng, M. Deng, N. Wang, Journal of The Electrochemical Society, 164 (2017) A438-A446. http://doi.org/10.1149/2.1211702jes
[21] Y. Feng, W. Xiong, J. Zhang, R. Wang, N. Wang, Journal of Materials Chemistry A, 4 (2016) 8658-8668. http://doi.org/10.1039/c6ta02574a.
[22] K.K. Alaneme, E.A. Okotete, Journal of Magnesium and Alloys, 5 (2017) 460-475. http://doi.org/10.1016/j.jma.2017.11.001.
[23] S. Yagi, A. Sengoku, K. Kubota, E. Matsubara, Corrosion Science, 57 (2012) 74-80. http://doi.org/10.1016/j.corsci.2011.12.032.
[24] J.W. Seong, W.J. Kim, Corrosion Science, 98 (2015) 372-381. http://doi.org/10.1016/j.corsci.2015.05.068.
[25] S.-M. Baek, H.J. Kim, H.Y. Jeong, S.-D. Sohn, H.-J. Shin, K.-J. Choi, K.-S. Lee, J.G. Lee, C.D. Yim, B.S. You, H.-Y. Ha, S.S. Park, Corrosion Science, 112 (2016) 44-53. http://doi.org/10.1016/j.corsci.2016.07.011.
[26] S.-H. Kim, J.U. Lee, Y.J. Kim, B.G. Moon, B.S. You, H.S. Kim, S.H. Park, Materials Science and Engineering: A, 703 (2017) 1-8. http://doi.org/10.1016/j.msea.2017.07.048.
[27] M. Deng, D. Höche, S.V. Lamaka, D. Snihirova, M.L. Zheludkevich, Journal of Power Sources, 396 (2018) 109-118. http://doi.org/10.1016/j.jpowsour.2018.05.090.
[28] N. Wang, R. Wang, C. Peng, Y. Feng, B. Chen, Corrosion Science, 64 (2012) 17-27. http://doi.org/10.1016/j.corsci.2012.06.024.
[29] L. Wang, R. Wang, Y. Feng, M. Deng, N. Wang, Jom, 69 (2017) 2467-2470. http://doi.org/10.1007/s11837-017-2276-z.
[30] N. Wang, R. Wang, C. Peng, Y. Feng, Corrosion Science, 81 (2014) 85-95. http://doi.org/10.1016/j.corsci.2013.12.005.
[31] N. Wang, Y. Mu, Q. Li, Z. Shi, RSC Advances, 7 (2017) 53226-53235. http://doi.org/10.1039/c7ra10652a
[32] F.W. Richey, B.D. McCloskey, A.C. Luntz, Journal of The Electrochemical Society, 163 (2016) A958-A963.
[33] Y. Zhao, G. Huang, C. Zhang, C. Peng, F. Pan, Materials Chemistry and Physics, 218 (2018) 256-261. http://doi.org/10.1016/j.matchemphys.2018.07.037

[34] M. Mayilvel Dinesh, K. Saminathan, M. Selvam, S.R. Srither, V. Rajendran, K.V.I.S. Kaler, Journal of Power Sources, 276 (2015) 32-38. http://doi.org/10.1016/j.jpowsour.2014.11.079.
[35] D. Höche, C. Blawert, S.V. Lamaka, N. Scharnagl, C. Mendis, M.L. Zheludkevich, Phys Chem Chem Phys, 18 (2016) 1279-1291. http://doi.org/10.1039/c5cp05577f.
[36] D. Höche, S.V. Lamaka, B. Vaghefinazari, T. Braun, R.P. Petrauskas, M. Fichtner, M.L. Zheludkevich, Sci Rep, 8 (2018) 7578. http://doi.org/10.1038/s41598-018-25789-8.
[37] Y. Li, J. Ma, G. Wang, F. Ren, Y. Zhu, Y. Song, Journal of The Electrochemical Society, 165 (2018) A1713-A1717. http://doi.org/10.1149/2.0581809jes].
[38] M.A. Deyab, Journal of Power Sources, 325 (2016) 98-103. http://doi.org/10.1016/j.jpowsour.2016.06.006.
[39] S.V. Lamaka, B. Vaghefinazari, D. Mei, R.P. Petrauskas, D. Höche, M.L. Zheludkevich, Corrosion Science, 128 (2017) 224-240. http://doi.org/10.1016/j.corsci.2017.07.011.
[40] D. Höche, S. Lamaka, M. Zheludkevich, EU patent EP3291361 A, 1 (2016).
[41] M.C. Lin, C.Y. Tsai, J.Y. Uan, Corrosion Science, 51 (2009) 2463-2472. http://doi.org/10.1016/j.corsci.2009.06.036.
[42] D. Cao, L. Wu, G. Wang, Y. Lv, Journal of Power Sources, 183 (2008) 799-804. http://doi.org/10.1016/j.jpowsour.2008.06.005.
[43] L. Fan, H. Lu, Journal of Power Sources, 284 (2015) 409-415. http://doi.org/10.1016/j.jpowsour.2015.03.063.
[44] G. Song, Advanced Engineering Materials, 7 (2005) 563-586. http://doi.org/10.1002/adem.200500013.
[45] E.L. Silva, S.V. Lamaka, D. Mei, M.L. Zheludkevich, ChemistryOpen, 7 (2018) 664-668. http://doi.org/10.1002/open.201800076.
[46] J.A. Dean, Lange's handbook of chemistry, New york; London: McGraw-Hill, Inc., 1999.
[47] A.E. Martell, R.M. Smith, Critical stability constants, Springer, 1974.
[48] R.M. Smith, A.E. Martell, Critical stability constants: second supplement, Springer, 1989.
[49] Y. Murakami, K. Nakamura, M. Tokunaga, Bulletin of the Chemical Society of Japan, 36 (1963) 669-675. http://doi.org/10.1246/bcsj.36.669
[50] V. Athavale, L. Prabhu, D. Vartak, Journal of Inorganic and Nuclear Chemistry, 28 (1966) 1237-1249. http://doi.org/10.1016/0022-1902(66)80450-5
[51] P. Jiang, C. Blawert, R. Hou, N. Scharnagl, J. Bohlen, M.L. Zheludkevich, Journal of Alloys and Compounds, 783 (2019) 179-192. http://doi.org/10.1016/j.jallcom.2018.12.296
[52] V. Shkirskiy, A.D. King, O. Gharbi, P. Volovitch, J.R. Scully, K. Ogle, N. Birbilis, Chemphyschem, 16 (2015) 536-539. http://doi.org/10.1002/cphc.201402666.
[53] R. Pinto, M.G.S. Ferreira, M.J. Carmezim, M.F. Montemor, Electrochimica Acta, 56 (2011) 1535-1545. http://doi.org/10.1016/j.electacta.2010.09.081.
[54] C. Daniel, J.O. Besenhard, Handbook of battery materials, John Wiley & Sons, 2012.
[55] X. Li, H. Lu, S. Yuan, J. Bai, J. Wang, Y. Cao, Q. Hong, Journal of The Electrochemical Society, 164 (2017) A3131-A3137. http://doi.org/10.1149/2.0971713jes
[56] M. Deng, R.-c. Wang, Y. Feng, N.-g. Wang, L.-q. Wang, Transactions of Nonferrous Metals Society of China, 26 (2016) 2144-2151. http://doi.org/10.1016/s1003-6326(16)64330-3.
[57] J. Li, K. Wan, Q. Jiang, H. Sun, Y. Li, B. Hou, L. Zhu, M. Liu, Metals, 6 (2016) 65. http://doi.org/10.3390/met6030065.
[58] D. Cao, X. Cao, G. Wang, L. Wu, Z. Li, Journal of Solid State Electrochemistry, 14 (2009) 851-855. http://doi.org/10.1007/s10008-009-0865-7.
[59] Y. Shi, C. Peng, Y. Feng, R. Wang, N. Wang, Journal of Alloys and Compounds, 721 (2017) 392-404. http://doi.org/10.1016/j.jallcom.2017.05.267.
[60] G. Marsh, E. Schaschl, Journal of the Electrochemical Society, 107 (1960) 960-965. http://doi.org/10.1149/1.2427579
[61] M. Andrei, F. Di Gabriele, P. Bonora, D. Scantlebury, Materials and corrosion, 54 (2003) 5-11. http://doi.org/10.1002/maco.200390010

[62] M. Deng, L. Wang, D. Höche, S.V. Lamaka, D. Snihirova, B. Vaghefinazari, M.L. Zheludkevich, Journal of Power Sources, 441 (2019) 227201. http://doi.org/10.1016/j.jpowsour.2019.227201.
[63] X. Liu, S. Liu, J. Xue, Journal of Power Sources, 396 (2018) 667-674. http://doi.org/10.1016/j.jpowsour.2018.06.085
[64] X. Liu, J. Xue, D. Zhang, Journal of Alloys and Compounds, (2019). http://doi.org/10.1016/j.jallcom.2019.07.151
[65] S. Yuan, H. Lu, Z. Sun, L. Fan, X. Zhu, W. Zhang, Journal of The Electrochemical Society, 163 (2016) A1181-A1187. http://doi.org/10.1149/2.0371607jes